Title

Suppression of connexin 43 phosphorylation promotes astrocyte survival and vascular regeneration in proliferative retinopathy

Journal

Proceedings of the National Academy of Sciences of the United States of America, 115(26)

ISSN

0027-8424

Authors

Slavi, Nefeli
Toychiev, Abduqodir H
Kosmidis, Stylianos
et al.

Publication Date

2018-06-26

DOI

10.1073/pnas.1803907115

Peer reviewed

Suppression of connexin 43 phosphorylation promotes astrocyte survival and vascular regeneration in proliferative retinopathy

Nefeli Slavi[a], Abduqodir H. Toychiev[a,1], Stylianos Kosmidis[b,1], Jessica Ackert[a], Stewart A. Bloomfield[a], Heike Wulff[c], Suresh Viswanathan[a], Paul D. Lampe[d], and Miduturu Srinivas[a,2]

[a]Department of Biological Sciences, State University of New York College of Optometry, New York, NY 10036; [b]Department of Neuroscience, Columbia University Medical Center, New York, NY 10032; [c]Department of Pharmacology, University of California, Davis, CA 95616; and [d]Translational Research Program, Fred Hutchinson Cancer Research Center, Seattle, WA 98109

Edited by Michael V. L. Bennett, Albert Einstein College of Medicine, Bronx, NY, and approved May 16, 2018 (received for review March 5, 2018)

Degeneration of retinal astrocytes precedes hypoxia-driven pathologic neovascularization and vascular leakage in ischemic retinopathies. However, the molecular events that underlie astrocyte loss remain unclear. Astrocytes abundantly express connexin 43 (Cx43), a transmembrane protein that forms gap junction (GJ) channels and hemichannels. Cx channels can transfer toxic signals from dying cells to healthy neighbors under pathologic conditions. Here we show that Cx43 plays a critical role in astrocyte apoptosis and the resulting preretinal neovascularization in a mouse model of oxygen-induced retinopathy. Opening of Cx43 hemichannels was not observed following hypoxia. In contrast, GJ coupling between astrocytes increased, which could lead to amplification of injury. Accordingly, conditional deletion of Cx43 maintained a higher density of astrocytes in the hypoxic retina. We also identify a role for Cx43 phosphorylation in mediating these processes. Increased coupling in response to hypoxia is due to phosphorylation of Cx43 by casein kinase 1δ (CK1δ). Suppression of this phosphorylation using an inhibitor of CK1δ or in site-specific phosphorylation-deficient mice similarly protected astrocytes from hypoxic damage. Rescue of astrocytes led to restoration of a functional retinal vasculature and lowered the hypoxic burden, thereby curtailing neovascularization and neuroretinal dysfunction. We also find that absence of astrocytic Cx43 does not affect developmental angiogenesis or neuronal function in normoxic retinas. Our in vivo work directly links phosphorylation of Cx43 to astrocytic coupling and apoptosis and ultimately to vascular regeneration in retinal ischemia. This study reveals that targeting Cx43 phosphorylation in astrocytes is a potential direction for the treatment of proliferative retinopathies.

retina | gap junctions | astrocytes | ischemia | neurovascular

Retinal vascular diseases, including retinopathy of prematurity (ROP) in children and proliferative diabetic retinopathy (PDR) in adults, are major causes of acquired blindness worldwide (1, 2). Initial stages of these diseases are characterized by inadequate perfusion of retinal areas due to either delayed vascular development (in ROP) or microvascular degeneration (in PDR) (3–6). The resulting hypoxia triggers endothelial cell proliferation, but the new vessels fail to effectively perfuse the ischemic areas of the retina. Instead, they form leaky neovascular tufts that grow into the preretinal space, leading to vision loss from intravitreal hemorrhage and retinal detachment. The processes of aberrant neovascularization and proper revascularization are influenced by several cell types, most notably retinal astrocytes (7–12). Studies in various animal models of retinopathy have shown that astrocytes degenerate in response to hypoxia, resulting in a sparse glial network in avascular retinal areas that is incapable of supporting proper revascularization (7, 13–18). Astrocyte loss also occurs in early stages of diabetes, where it is associated with increased permeability of the blood–retinal barrier (19, 20).

The molecular events that underlie astrocyte degeneration in ischemic retinopathies remain unclear. Astrocytes are extensively coupled via gap junction (GJ) channels formed by connexin 43 (Cx43). GJ channels can mediate the exchange of metabolites and can transmit signaling but can also act as conduits for the movement of cytotoxic molecules from dying cells to their coupled neighbors, thereby expanding hypoxia-induced focal damage (21, 22). In the brain, increases in GJ coupling between reactive astrocytes occur following stroke and epileptiform activity leading to amplification of injury (23, 24). Cx43 can also form unopposed hemichannels, which allow direct communication between cell cytoplasm and extracellular space. Cx43 hemichannel activity has also been reported to increase in response to ischemia of the brain and retina, spinal cord injury, and stroke, leading to propagation of secondary cell death through release of cytotoxic mediators (22, 25–27).

Here we identify a key role for Cx43 in astrocyte degeneration in a mouse model of oxygen-induced retinopathy (OIR), a well-established animal model of ROP that also recapitulates many features of pathologic neovascularization seen in proliferative DR in humans (28–30). We demonstrate that genetic deletion or

Significance

Vascular regeneration during retinal ischemia is critical for curtailing hypoxia-driven aberrant neovascularization and neuronal damage. Apoptotic cell death of astrocytes is a key initiating factor for improper vascular growth. Here we report that astrocytic connexin (Cx43) gap junction (GJ) channels are major contributors to astrocyte degeneration and vascular remodeling that follow tissue ischemia. Astrocyte apoptosis is due to phosphorylation of Cx43 by casein kinase 1δ (CK1δ), which in turn leads to an increase in GJ coupling and amplification of injury. Deletion of Cx43 or inhibition of its phosphorylation by CK1δ rescues astrocytes and leads to restoration of a functional vasculature in the retina, while reducing neovascularization and improving neuroretinal function, thereby providing viable options for the treatment of ischemic retinopathies.

Author contributions: N.S. and M.S. designed research; N.S., A.H.T., S.K., and P.D.L. performed research; J.A., H.W., and P.D.L. contributed new reagents/analytic tools; J.A. set up the oxygen-induced retinopathy model; S.A.B. provided electrophysiology expertise; S.V. guided electroretinogram recordings and assisted with data analysis; N.S. analyzed data; and N.S. and M.S. wrote the paper.

The authors declare no conflict of interest.

This article is a PNAS Direct Submission.

[1]A.H.T. and S.K. contributed equally to this work.

[2]To whom correspondence should be addressed. Email: msrinivas@sunyopt.edu.

This article contains supporting information online at www.pnas.org/lookup/suppl/doi:10.1073/pnas.1803907115/-/DCSupplemental.

Published online June 11, 2018.

pharmacological inhibition of Cx43 channels protects the astrocyte network and enhances revascularization into ischemic areas of the retina, thereby suppressing aberrant neovascularization and resulting in improved neuroretinal function. We also explore the mechanism by which Cx43 contributes to astrocyte loss. Phosphorylation of astroglial Cx43, a key process regulating the protein's function (31–33), is markedly enhanced soon after exposure to hypoxia, which is accompanied by an increase in astrocytic GJ coupling at time points before astrocyte loss. Cx43 phosphorylation was found to be mediated by CK1δ, a kinase whose role in ischemic retinopathies has not been described previously. Last, our results show that reparative angiogenesis can be attained via inhibition of Cx43 phosphorylation by CK1δ. These results mechanistically link Cx43 phosphorylation to channel function, astrocyte survival, and retinal vascular remodeling.

Results

Deletion of Cx43 from Astrocytes Does Not Alter Retinal Structure and Function. We first examined the expression of Cx43 protein in the developing retina of room-air raised mice (*SI Appendix*, Figs. S1 and S2). In vertical retinal sections obtained from WT mice ($Cx43^{flox}$) at P13, Cx43 punctate staining was detected in the proximal side of the ganglion cell layer (GCL), where astrocytes reside, and in the retinal pigment epithelium (RPE). In the inner retina, Cx43 staining was localized exclusively to GFAP-positive cells, which are mainly astrocytes as Müller glia do not express GFAP under normal conditions (*SI Appendix*, Fig. S1*A*). In comparison, Cx43 puncta were virtually absent in retinas in which Cx43 was genetically deleted from GFAP-expressing cells ($Cx43^{aKO}$). We did not detect Cx43 labeling in the inner nuclear (INL) or inner plexiform (IPL) layers at this developmental time point or any colocalization with CRALBP, a specific marker of Müller cells (*SI Appendix*, Fig. S1). These results are consistent with previous studies showing that Müller cells in mammalian retinas have limited GJ channel connectivity (34–36).

Intense staining of Cx43 in GFAP-expressing astrocytes can be observed in retinal whole-mount preparations from $Cx43^{flox}$ mice (*SI Appendix*, Fig. S2*A*). Deletion of astrocytic Cx43 led to a strong decrease in Cx43 labeling. Cx43 puncta were also infrequently seen on isolectin B4-stained vessels of the superficial plexus. The expression of the protein in blood vessels was better visualized in the absence of astrocytic Cx43 (*SI Appendix*, Fig. S2*A*). Overall, the ablation of astrocytic Cx43 resulted in a substantial reduction in the total amount of the protein compared with that in $Cx43^{flox}$ retinas, confirming that astrocytes are the main source of Cx43 in the developing mouse retina (*SI Appendix*, Fig. S2*B*).

We also found that GJ coupling between astrocytes is completely reduced by deletion of Cx43. Dye-transfer studies using the GJ-permeable tracer Neurobiotin confirmed that GJ channels extensively couple retinal astrocytes in $Cx43^{WT}$ mice (*SI Appendix*, Fig. S2 *C* and *D*). In contrast, tracer coupling between astrocytes was completely lost in $Cx43^{aKO}$ retinas, indicating that Cx43 is the only connexin isoform expressed in these cells.

The inability of astrocytes to form a coupled network in $Cx43^{aKO}$ retinas did not affect angiogenesis during early postnatal development. $Cx43^{flox}$ and $Cx43^{aKO}$ retinas showed similar degrees of vascularization at P5 (*SI Appendix*, Fig. S3*A*). All three plexuses of the inner vascular network had normal appearance and branching by P17 (*SI Appendix*, Fig. S3 *B* and *C*) in $Cx43^{aKO}$ mice. The absence of Cx43 also did not affect the structure and function of the neural retina. Morphometric analysis of vertical retinal sections labeled with DAPI showed no changes in the thickness of the outer and inner nuclear layers (*SI Appendix*, Fig. S3*D*) or in the number of cells that reside at the GCL (*SI Appendix*, Fig. S3*E*). Consistent with these histological findings, electroretinograms (ERG) showed that scotopic a- and b-wave amplitudes and oscillatory potentials (OPs) of $Cx43^{aKO}$ retinas were not significantly different from $Cx43^{flox}$ retinas (*SI Appendix*, Fig. S3 *F–I*).

Cx43 Deletion Rescues Astrocytes from Hypoxia-Induced Damage in the Mouse OIR Model. To study the role of Cx43 in the hypoxic retina, we used the OIR mouse model (Fig. 1*A*). In this model, hypoxia causes a decrease in the density of astrocytes that reside in the central avascular areas by P14. We considered the possibility that Cx43 can negatively affect the density of the retinal astrocyte network through its involvement in secondary cell death. Thus, we exposed $Cx43^{flox}$ and $Cx43^{aKO}$ mice to OIR and evaluated the density of retinal astrocytes during hypoxia. GFAP-positive cell bodies corresponding to astrocytes were counted in the superficial vascular plexus of retinal whole mounts. Our measurements did not include reactive Müller cells, which also express GFAP, because their cell bodies are located in the INL and not the proximal side of the GCL. At P12, no significant differences in the populations of astrocytes were observed between $Cx43^{flox}$ and $Cx43^{aKO}$ retinas (Fig. 1*C*). At P14, $Cx43^{flox}$ retinas were mostly devoid of astrocytes in their center (Fig. 1*B*), as expected (7, 17). In contrast, a significantly higher density of astrocytes was found in central, hypoxic regions of $Cx43^{aKO}$ retinas compared with that in $Cx43^{flox}$ littermates (Fig. 1 *B* and *C*). The peripheral astrocytes remained at high densities in both groups (Fig. 1*B*). These results suggest that in OIR, Cx43 expressed in astrocytes impairs the astroglial network and deprives the retina of a proper scaffold necessary for directional angiogenesis.

Next, we assessed apoptotic cell death in hypoxic astrocytes in $Cx43^{flox}$ and $Cx43^{aKO}$ OIR retinas using Annexin V labeling at P13, a time point preceding the peak of astrocyte degeneration (P14). Annexin V-positive cells were prevalent in the central, hypoxic retina of $Cx43^{flox}$ mice (*SI Appendix*, Fig. S4), in agreement with previous studies (17). In contrast, there were fewer apoptotic cells in $Cx43^{aKO}$ retinas, further supporting the notion that GJs play a role in astrocytic cell death.

Cx43 Deletion in Astrocytes Promotes Reparative Angiogenesis in OIR. Preservation of the astrocyte network is correlated with accelerated regrowth of retinal blood vessels and reduced intravitreal neovascularization (7, 16). Therefore, we tested the involvement of Cx43 in vascular remodeling in OIR by staining $Cx43^{flox}$ and $Cx43^{aKO}$ retinas with isolectin and quantifying the avascular and neovascular areas at P12, P14, and P17 (Fig. 2). Upon return to ambient air at P12, both $Cx43^{flox}$ and $Cx43^{aKO}$ retinas suffered significant but comparable central vasoobliteration (Fig. 2 *A* and *B*), indicating that astrocytic Cx43 does not participate in vessel regression that occurs during exposure to high oxygen. However, when examined at P14, vasoobliterated areas in $Cx43^{aKO}$ retinas were significantly smaller compared with $Cx43^{flox}$ retinas (Fig. 2 *C* and *D*), indicative of accelerated revascularization. This enhanced vascular regeneration in the absence of Cx43 became even more profound at P17. $Cx43^{aKO}$ mice showed higher recovery from retinal vasoobliteration compared with $Cx43^{flox}$ and $Cx43^{fl/+}$ (heterozygous) littermates (Fig. 2 *E* and *F*). Intravitreal neovascularization was also markedly suppressed in $Cx43^{aKO}$ retinas (Fig. 2 *E* and *G*). These results demonstrate that Cx43 expressed in astrocytes contributes to the progression of abnormal vessel growth triggered by hypoxic stress, whereas conditional deletion of Cx43 from astrocytes promotes directional angiogenesis in the ischemic retina.

To determine whether the newly formed vessels in the central retina of $Cx43^{aKO}$ mice were functional, hypoxic areas of the tissue were quantified using a fluorescent Hypoxyprobe assay. We detected complete and restricted overlap between avascular and hypoxic areas for both $Cx43^{flox}$ and $Cx43^{aKO}$ retinas. However, the hypoxic retinal regions of $Cx43^{aKO}$ mice were significantly reduced compared with their control littermates (Fig. 2 *H*

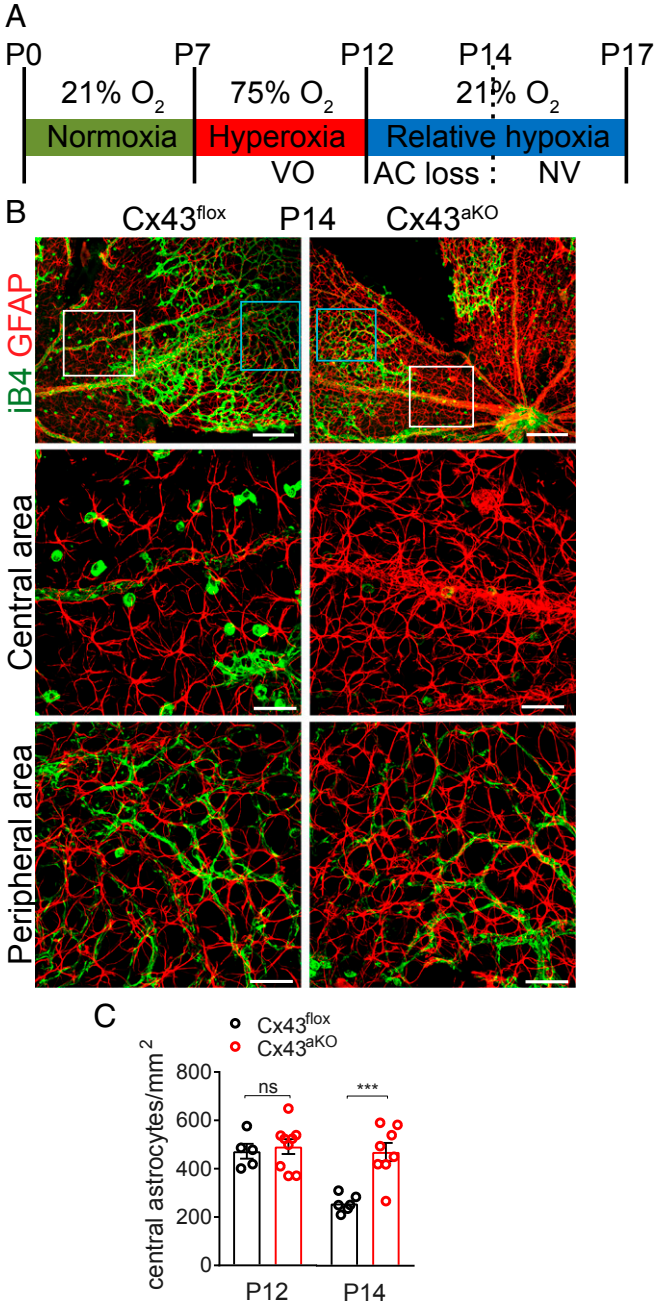

Fig. 1. Conditional deletion of Cx43 preserves the astrocytic network in OIR. (*A*) Schematic of the mouse model of OIR. Neonatal mice are exposed to 75% O_2 from P7 to P12. Hyperoxia results in vasoobliteration in the central retina (see Fig. 2 for images). Mice return to room air (21% O_2) at P12, and the retina becomes immediately hypoxic due to the absence of central vasculature. The hypoxic phase (between P12 and P17) is characterized by partial revascularization and neovascular tuft formation, which commences at P14 and peaks at P17. Decrease in the density of astrocytes is also observed during hypoxia, between P12 and P14–P15. (*B*) (*Top*) Representative images of whole-mount $Cx43^{flox}$ and $Cx43^{aKO}$ retinas in OIR stained with isolectin (green) and anti-GFAP (red) at P14. (Scale bars: 200 μm.) (*Middle* and *Bottom*) Higher-magnification images from the boxed areas, corresponding to the central and peripheral retinal regions, respectively. (Scale bars: 50 μm.) (*C*) Quantification of astrocytes present in the avascular areas of $Cx43^{flox}$ and $Cx43^{aKO}$ retinas in OIR at P12 (n = 5–9) and P14 (n = 6–8). At P14, deletion of Cx43 led to ∼1.8-fold increase in the GFAP-labeled astrocytes in the avascular retinal regions compared with control. Data are presented as mean ± SEM. Student's t test, ns $P > 0.05$, ***$P < 0.001$.

and *I*), suggesting that the regenerated vascular plexus in these mice has the capacity to reperfuse and minimize ischemic injury.

$Cx43^{aKO}$ Mice Demonstrate Improved Neuroretinal Function. We next determined whether the reduction of overall retinal hypoxia in $Cx43^{aKO}$ mice led to changes in neuronal responses to light stimuli. OIR is associated with a depression in inner neuroretinal function, which is mainly manifested as a decrease in the amplitude of the b wave and OPs in ERG (37, 38). In agreement with these previous ERG reports, $Cx43^{flox}$ mice exposed to OIR showed reduced bipolar and amacrine cell scotopic responses (Fig. 3). Deletion of astrocytic Cx43 partially, yet significantly, restored these responses (Fig. 3*A*), as demonstrated by enhanced rod-driven b-wave amplitudes (Fig. 3*B* and *SI Appendix*, Fig. S5*A*) and OPs (Fig. 3*C*). The slope and semisaturation constant of the b-wave intensity response function as well as the b-wave time-to-peak did not differ significantly between the two groups (*SI Appendix*, Fig. S5).

Pharmacological Inhibition of Cx43 Channel Function Accelerates Vascular Regeneration and Suppresses Pathologic Angiogenesis. To support our results on the involvement of Cx43 in pathologic angiogenesis, we inhibited Cx43 channels pharmacologically during the hypoxic phase of OIR. Connexin mimetic peptides are effective at blocking Cx43 hemichannels with high potency; however, inhibition of cell–cell GJ coupling requires much higher concentrations (26, 39, 40). These peptides can also alter expression of Cx43 (41). Therefore, Cx43 channel blockade was achieved by intravitreal administration of SBO15 (*SI Appendix*, Fig. S6*A*), a novel isoquinoline-based compound that was originally synthesized for studies on voltage-gated K^+ channels (42). We chose SBO15 because our results in expression systems indicated that the compound selectively inhibits Cx43 GJ channels (IC_{50} ∼ 2 μM and maximal inhibition ∼10–20 μM) without affecting those formed by connexins in retinal neurons (e.g., Cx36) (*SI Appendix*, Fig. S6).

We injected intravitreally SBO15 (20 μM) in WT OIR retinas at P12 and monitored changes to the vasculature during the hypoxic phase. SBO15 led to a significant improvement in vasoobliteration and neovascularization seen at P17 compared with PBS-treated animals (Fig. 4 *A*–*C*). Consistent with results obtained from $Cx43^{aKO}$ mice, inhibition of Cx43 channels also enhanced vascular regrowth by P14 (Fig. 4*B*). Central revascularization led to protection against neovascularization as indicated by the suppression of neovascular tuft formation as early as P15 (Fig. 4*C*). Besides its effects on the vasculature, SBO15 treatment significantly improved the density of astrocytes in the hypoxic retina at P14 (Fig. 4 *D* and *E* and *SI Appendix*, Fig. S6*D*). The increase in astrocyte numbers caused by SBO15 was comparable to that found in $Cx43^{aKO}$ mice. These pharmacological experiments indicate that the loss of central astrocytes and vascular remodeling are due to the channel-dependent function of Cx43.

Cx43-Mediated Astrocytic GJ Coupling Is Elevated During the Early Hypoxia Phase. Cx43 can function as unopposed hemichannels or as intercellular GJ channels. Opening of either channel configuration in pathologic conditions has been implicated in secondary cell death following focal damage (21, 22, 25–27). To determine whether retinal hypoxia is associated with changes in the channel function of astrocytic Cx43, we monitored the activity of Cx43 hemichannels and GJ channels at the onset of hypoxia at P12 and at different time points until P14 (Fig. 5), when changes in astrocyte density were maximal.

Cx43 hemichannel activity was assayed using ex vivo uptake of ethidium bromide (EtBr). EtBr was found to localize within cell bodies of numerous cells, including GFAP-expressing cells. However, no significant change in the number of EtBr-labeled astrocytes was observed during the first 24 h of hypoxia (Fig. 5 *A* and *B*). Additionally, EtBr labeling was not reduced in the

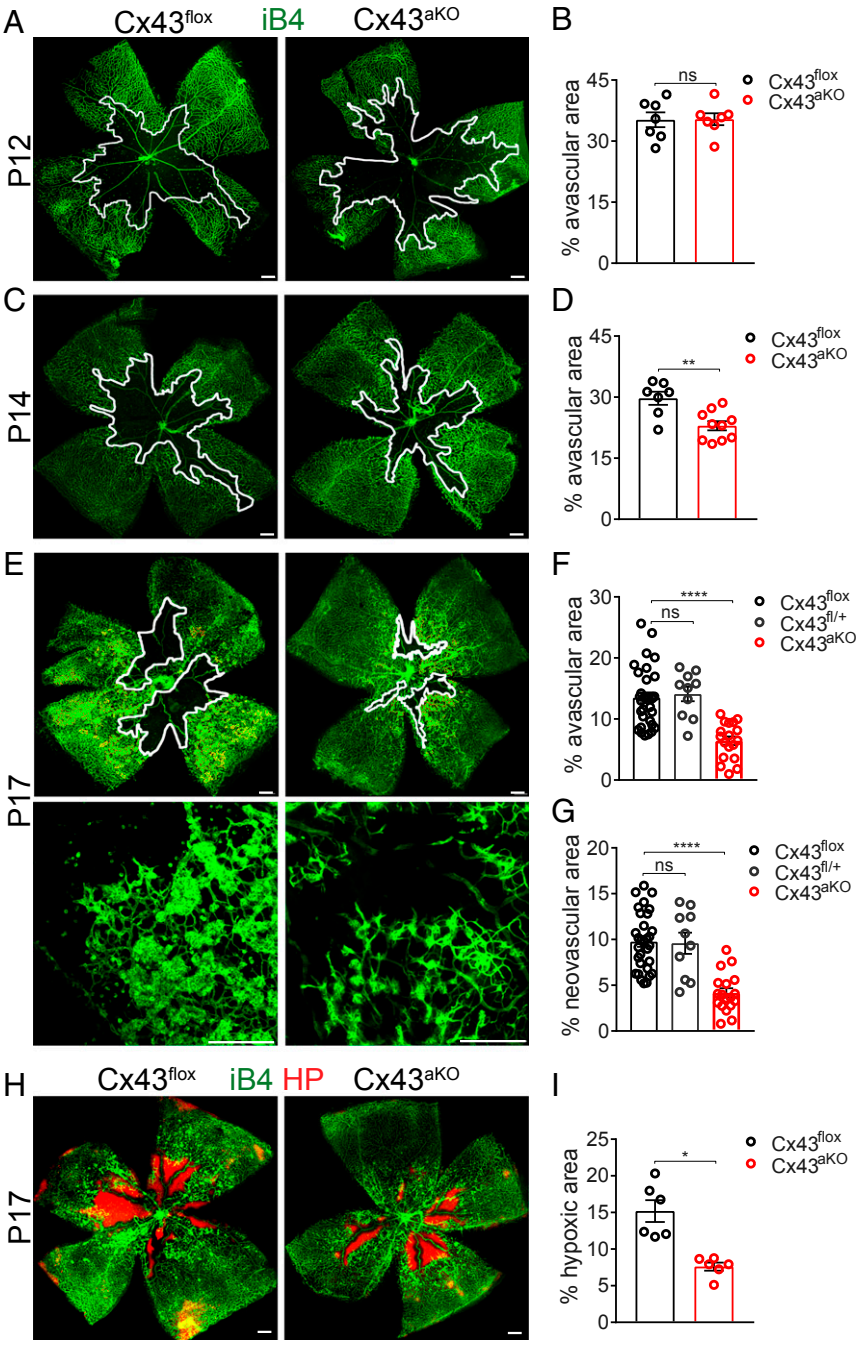

Fig. 2. Deletion of astrocytic Cx43 promotes reparative angiogenesis and reduces hypoxia in OIR. Representative images of whole-mount $Cx43^{flox}$ and $Cx43^{aKO}$ retinas in OIR stained with isolectin (green) at (*A*) P12, (*C*) P14, and (*E*) P17. White lines indicate the border of the avascular area in each retina. Images of neovascular tufts at P17 are illustrated in *E* (*Bottom*). Quantification of the avascular areas of $Cx43^{flox}$ and $Cx43^{aKO}$ retinas in (*B*) P12 (n = 7–7), (*D*) P14 (n = 7–9), and (*F*) P17 (n = 18–21). $Cx43^{aKO}$ retinas exhibited accelerated revascularization compared with $Cx43^{flox}$. (*G*) Quantification of the retinal areas covered with neovascular tufts at P17 revealed a reduction in neovascularization of $Cx43^{aKO}$ (n = 21) retinas compared with $Cx43^{flox}$ (n = 18). (*H* and *I*) Representative images of whole-mount $Cx43^{flox}$ (n = 6) and $Cx43^{aKO}$ (n = 6) retinas in OIR stained with isolectin (green) and Hypoxyprobe (red) at P17 and quantification of the hypoxic areas. $Cx43^{aKO}$ retinas were significantly less hypoxic compared with $Cx43^{flox}$. Data are presented as mean ± SEM. Student's t test, ns $P > 0.05$, *$P < 0.05$, **$P < 0.01$, ****$P < 0.0001$. (Scale bars: 250 μm.)

presence of Gap19 peptide, a selective inhibitor of Cx43 hemichannels (43) (Fig. 5*B*), indicating that EtBr uptake was likely unrelated to Cx43 hemichannel opening.

Although hypoxia did not affect hemichannel activity, it had a significant effect on GJ coupling between astrocytes within the ischemic regions of the retina. Individual astrocytes were loaded with the GJ-permeant tracer Neurobiotin, whose intercellular spread was used to assay astrocytic coupling. Immediately after the return of animals to room air at P12 (0 h hypoxia), astrocytes of the central retina were only weakly coupled. Within 6 h, however, there was a threefold increase in the number of Neurobiotin-positive astrocytes, indicative of an extensively coupled network (Fig. 5 *C*–*E*). Astrocytic coupling remained elevated for the next 24 h and then gradually decreased, likely due to degeneration of astrocytes in hypoxic areas. The change in GJ coupling was restricted to the avascular areas of the retina. In the peripheral vascularized retina, there was no difference in the number of coupled astrocytes throughout the same period (Fig. 5 *D* and *E*), indicating that hypoxia provides the trigger for the increase in GJ channels function. At all of the time points, $Cx43^{aKO}$ astrocytes were not coupled to each other, as expected (*SI Appendix*, Fig. S7*A*). In addition, we rarely observed transfer of Neurobiotin from the GCL to the INL. Even when Neurobiotin labeling was detected occasionally in the INL, it did not colocalize with GFAP-expressing Müller cells, ruling out the possibility that astrocytes-to-Müller cells coupling is induced by hypoxia (*SI Appendix*, Fig. S7 *B* and *C*).

Cx43 Becomes Phosphorylated During the Early Hypoxic Phase of OIR. Elevated astrocytic coupling early in the hypoxic phase of OIR could be attributed to increased Cx43 expression. However,

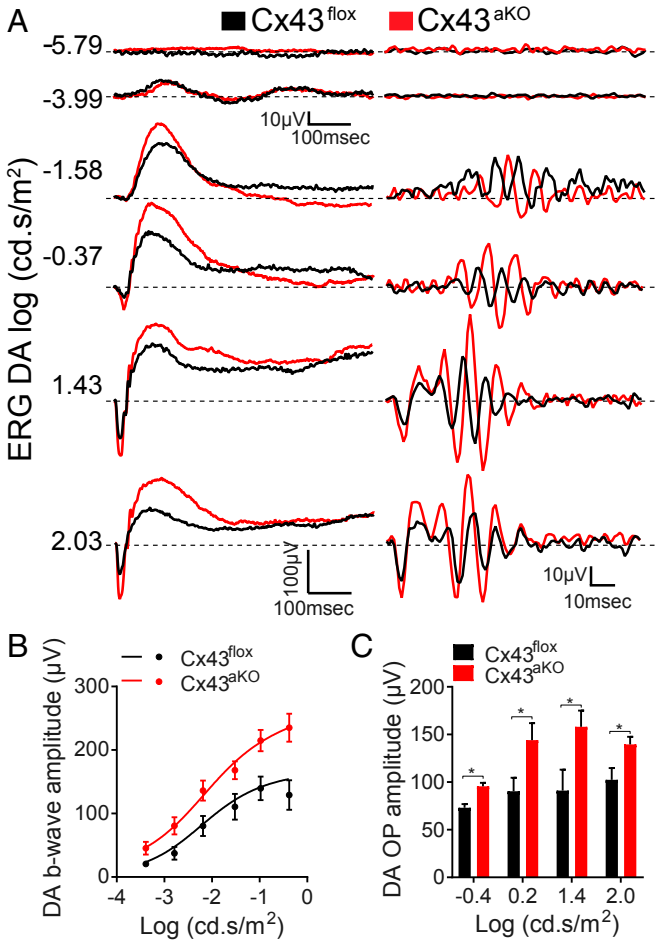

Fig. 3. Deletion of astrocytic Cx43 improves neuroretinal function in OIR. (*A*) Recordings of (*Left*) a and b waves and (*Right*) OPs of scotopic ERGs in response to different stimulus intensities from $Cx43^{flox}$ and $Cx43^{aKO}$ mice exposed to OIR. Light intensities in log scot. cd s/m^2 are shown to the left of each trace. (*B* and *C*) $Cx43^{aKO}$ mice showed a significant improvement in function of the neural retina. (*B*) Quantification of the amplitudes of the scotopic b wave and (*C*) summed OPs at different stimulus intensities. Lines in *B* represent the fit of the Naka Rushton equation to the data. Data are presented as mean ± SEM (n = 5 each of $Cx43^{flox}$ and $Cx43^{aKO}$ mice). Student's t test, *$P < 0.05$.

protein analysis of retinas isolated from WT mice in OIR indicated that Cx43 protein levels were not significantly up-regulated during vascular remodeling (Fig. 6 *A* and *B*). Cx43 appeared to undergo noticeable changes in phosphorylation state during the first 24 h in hypoxia. Immediately after introduction to hypoxia (0 h hypoxia), retinal Cx43 was present mostly as a 40 kDa protein (referred to as P0 form). However, Cx43 isoforms were also detected at 41 and 43 kDa after 6 h. These correspond to differentially phosphorylated forms of the protein [referred to as P1 and P2 forms, respectively (33)]. More specifically, the P2 form was increased by threefold and remained at high levels at 24 h (Fig. 6 *A* and *B*). Notably, the observed changes in Cx43 phosphorylation were temporally correlated with the changes in astrocytic coupling (Figs. 5*D* and 6*B*).

Cx43 is also expressed in endothelial cells (40, 44). Therefore, to determine whether hypoxia triggers the phosphorylation of Cx43 in astrocytes, endothelial cells or both, we compared the expression and phosphorylation patterns of the protein between $Cx43^{flox}$ and astrocyte-specific ($Cx43^{aKO}$) and endothelial cell-specific ($Cx43^{eKO}$) Cx43 KO retinas. $Cx43^{aKO}$ retinal lysates displayed a near absence of all Cx43 forms at 6 h of hypoxia (Fig. 6 *C* and *D*). In contrast, both total Cx43 and P2-Cx43 levels in $Cx43^{eKO}$ lysates were unchanged compared with $Cx43^{flox}$ retinas (Fig. 6 *C* and *D*). We also considered whether reactive Müller

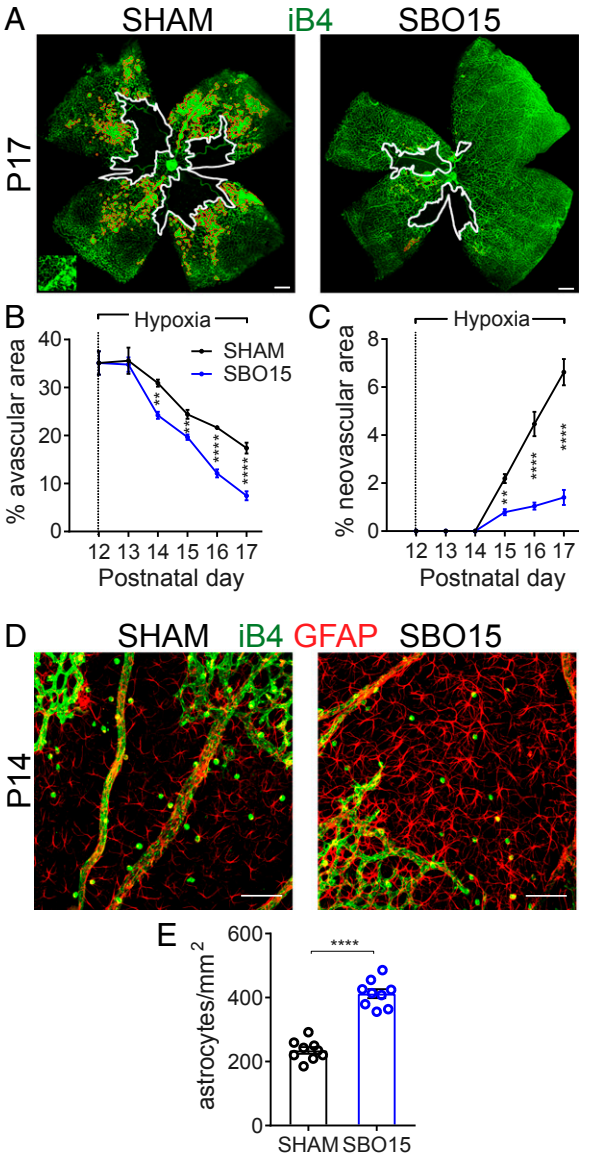

Fig. 4. Pharmacological inhibition of channels formed by Cx43 early in the hypoxic phase of OIR promotes reparative angiogenesis. (*A*) Representative images of isolectin-stained WT retinas at P17 injected intravitreally with PBS (SHAM) or with 20 μM SBO15 at P12. The borders of the avascular areas are outlined by white lines, and the neovascular tufts are marked by red lines. Injection of SBO15 reduced both the avascular and neovascular areas. (Scale bars: 250 μm.) The reduction in (*B*) avascular and (*C*) neovascular areas relative to the total retinal area was measured between P12 and P17 during the hypoxic phase of OIR after a single intravitreal injection of SBO15 at P12 (n = 3–9). SBO15 accelerated revascularization as early as P14 and reduced neovascularization between P14 and P17. (*D*) Representative images of isolectin- and GFAP-stained whole-mount WT retinas at P14, injected intravitreally with PBS or with 20 μM SBO15 at P12. High magnification images from the central and peripheral retinal regions are shown in *SI Appendix*, Fig. S5*B*. (Scale bars: 100 μm.) (*E*) Quantification of astrocytes present in the avascular areas of SHAM (n = 9) and SBO15-treated retinas (n = 9) in OIR at P14. SBO15 led to ~1.7-fold increase in the GFAP-labeled astrocytes in the avascular retinal regions compared with control. Data are presented as mean ± SEM. Student's t test, ns $P > 0.05$, *$P < 0.05$, **$P < 0.01$, ***$P < 0.001$, ****$P < 0.0001$.

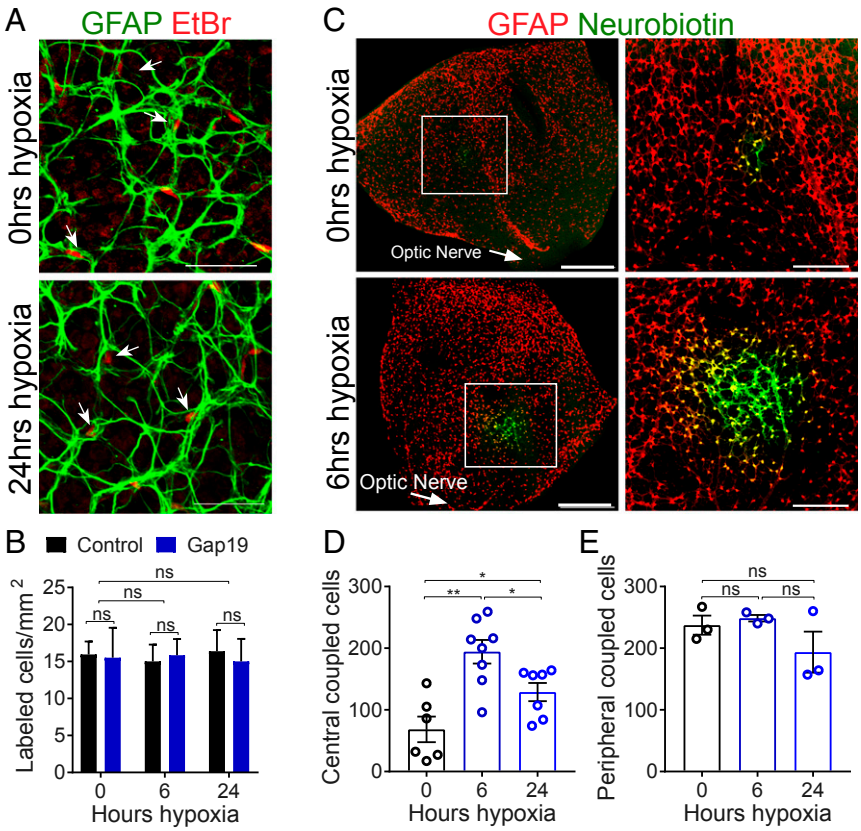

Fig. 5. Cx43 GJ coupling but not hemichannel activity in astrocytes is elevated during hypoxia in OIR. (*A*) Hemichannel activity as measured by ethidium bromide (EtBr) uptake in astrocytes. Images of whole-mount retinas incubated with EtBr (red) and labeled with anti-GFAP (green) after 0 and 24 h during the hypoxic phase of OIR. Arrows indicate the uptake of EtBr into cell bodies of astrocytes. (Scale bars: 50 μm.) (*B*) The number of cells with tracer uptake normalized to retinal area was measured in the absence (control) or in the presence of Cx43 hemichannel-selective inhibitor, Gap19 (300 μM) at 0 ($n = 5$–8), 6 ($n = 3$–4), and 24 h ($n = 4$–9) of hypoxia. Tracer uptake was similar at all three time points and was not blocked by Gap19. (*C*) GJ coupling between astrocytes of tdTomato^{GFAP} mice (red) was visualized by diffusion of Neurobiotin (green) introduced into a single astrocyte at 0 and 6 h in hypoxia. (*Left*) Images at 4× magnification at each time point. (Scale bars: 500 μm.) (*Right*) Higher magnification of the boxed areas. (Scale bars: 250 μm.) (*D* and *E*) Quantification of astrocytes labeled with Neurobiotin after 0, 6, and 24 h of hypoxia in the central ($n = 6$–8) and peripheral ($n = 3$) retina showed an increase in astrocytic coupling in hypoxia. Data are presented as mean ± SEM. Two-way ANOVA is used in *B*. One-way ANOVA is used in *D* and *E*. ns $P > 0.05$, *$P < 0.05$, **$P < 0.01$.

cells express Cx43. Expression of GFAP in Müller glia was detected in the central retina after 24 h (P13) of hypoxia, but not at 6 h of hypoxia (P12) (*SI Appendix*, Fig. S8 *A* and *B*), in agreement with previous studies (12). No reactive Müller glia were seen in the peripheral regions. In both the central and peripheral retinal areas, Cx43 expression was localized to the GCL, around nuclei corresponding to astrocytes (*SI Appendix*, Fig. S8 *B* and *C*). Little or no Cx43 was seen in cell bodies of Müller cells or their processes in other retinal layers. Together, these results demonstrate that the distinct phosphorylation patterns correspond to astrocytic Cx43 and not Cx43 present in other cells types.

CK1δ Phosphorylates Cx43 at Ser325/328/330 to Induce Changes in Astrocytic GJ Coupling. The C terminus of Cx43 contains several phosphorylation sites; depending on the targeted residue, phosphorylation of Cx43 can result in enhanced intracellular trafficking, channel assembly and increased GJ communication, or in protein internalization and degradation, and thereby reduced coupling (33, 45, 46). Thus, it was of interest to determine which of the C-terminal residues account for the differential phosphorylation of Cx43 in response to hypoxia. Retinal lysates were immunoblotted using various phosphospecific antibodies. A dramatic increase in the Ser325/328/330-phosphorylated Cx43, coinciding with the P2 fraction, was observed after 6 h of hypoxia compared with the onset of hypoxia (Fig. 6 *E* and *F*). We also examined the phosphorylation pattern of Cx43 in retinal lysates from Ser325/328/330 phosphorylation-deficient mice (Cx43^{S3A}) and found minimal amounts of P2_Cx43 after 6 h in hypoxia (Fig. 6 *G* and *H*), substantiating that changes in Cx43 conformation were due to phosphorylation of Ser325/328/330.

Cx43 is recognized as a substrate by several kinases (33, 46). Phosphorylation at Ser325/S328/S330 is mediated by CK1δ (47–49). We injected intravitreally a highly selective CK1δ inhibitor (PF670462, 1 μM) at the onset of hypoxia in OIR. PF670462 led to a gradual reduction of the P2 fraction of Cx43 (Fig. 6 *I* and *J*), bringing it to almost baseline levels within 9 h. This result verified that CK1δ phosphorylates Cx43 during the hypoxic phase of OIR.

CK1δ phosphorylation of Cx43 is known to increase the assembly of Cx43 channels into GJ plaques (47, 48). Therefore, we investigated whether phosphorylation of Cx43 by CK1δ is responsible for the increase in GJ coupling seen in hypoxia. Indeed, inhibition of CK1δ upon intravitreal administration of PF670462 prevented the increase in astrocytic coupling seen during hypoxia (*SI Appendix*, Fig. S9 *A* and *B*). Consistent with these findings, cell pairs expressing WT Cx43 in vitro exhibited significantly higher coupling compared with cell pairs expressing Cx43_S325A/S328A/S330A or compared with those treated with PF670462 (*SI Appendix*, Fig. S9*C*).

Inhibition of Cx43 Ser325/328/330 Phosphorylation Enhances Retinal Revascularization and Ameliorates Pathologic Neovascularization. Having established a causal relationship between phosphorylation of Ser325/328/330 by CK1δ and robust GJ intercellular coupling,

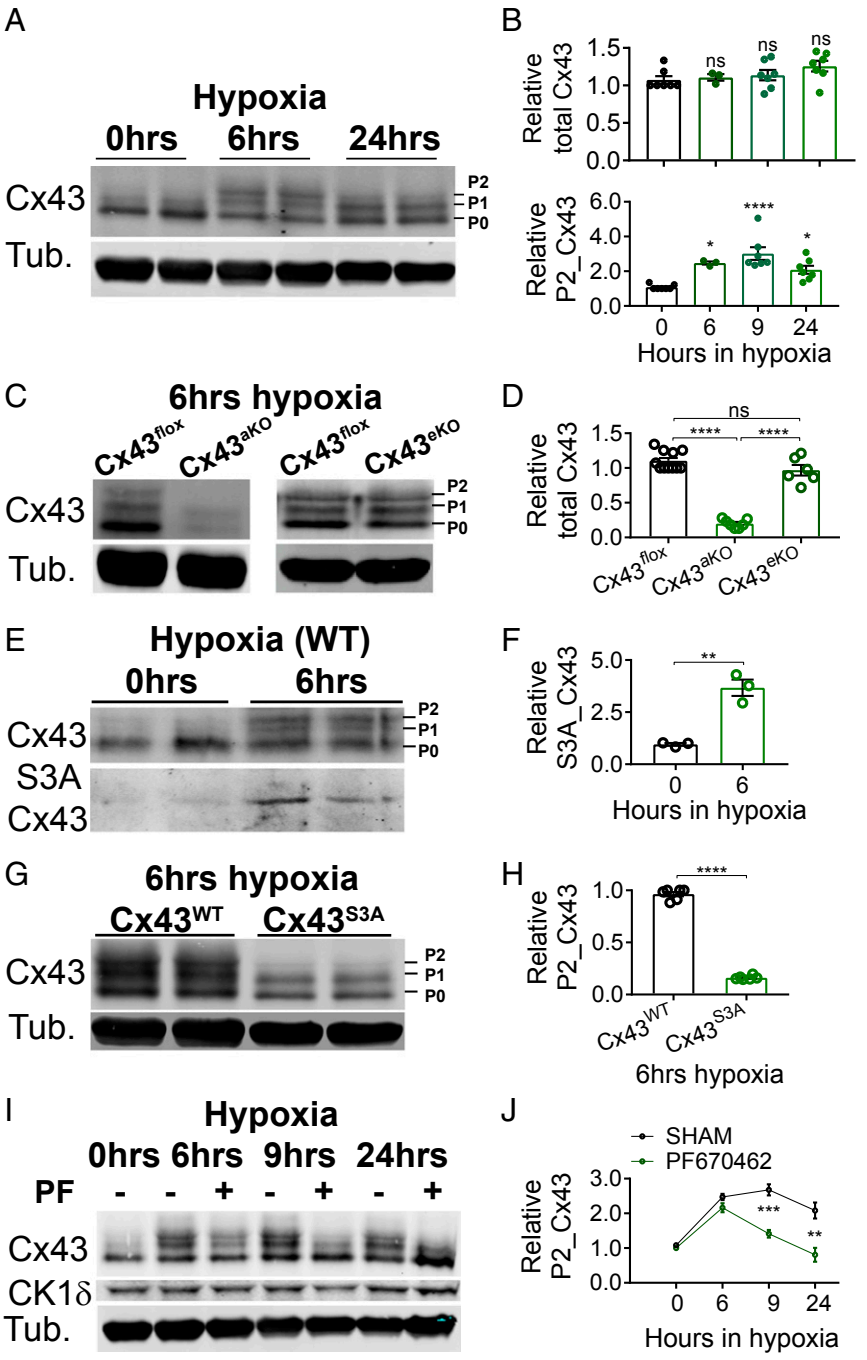

Fig. 6. Cx43 becomes phosphorylated at Ser325/328/330 by CK1δ during hypoxia. (*A*) Western blot of Cx43 in WT retinas at 0, 6, and 24 h hypoxia, showing a large increase in the P2 phosphorylated form of Cx43 within 6 h. (*B*) Quantification of (*Top*) total Cx43 or (*Bottom*) the P2 form normalized to tubulin at 6 ($n = 3$), 9 ($n = 7$), and 24 h ($n = 7$) relative to 0 h ($n = 7$). (*C* and *D*) Western blot and quantification of total Cx43 in control ($Cx43^{flox}$) ($n = 11$), astrocyte- ($Cx43^{aKO}$) ($n = 7$), and endothelial cell- ($Cx43^{eKO}$) ($n = 6$) specific knockout retinas at 6 h posthypoxia. Majority of retinal Cx43 is present in astrocytes. (*E* and *F*) Western blot and quantification of Ser325/328/330-phosphorylated Cx43 at 0 and 6 h in hypoxia. The phosphospecific antibody recognized a signal corresponding to the P2_Cx43 (~43 kDa) ($n = 3$). (*G*) Western blot of Cx43 in $Cx43^{WT}$ and $Cx43^{S3A}$ retinas at 6 h in hypoxia. (*H*) Quantification of P2_Cx43 levels in $Cx43^{WT}$ ($n = 6$) and $Cx43^{S3A}$ retinas ($n = 6$). (*I*) Western blot of Cx43 at different time points in hypoxia following intravitreal injection of PBS (–) or the CK1δ inhibitor PF670462 (+). PF670462 reduced P2_Cx43. (*J*) Quantification of P2_Cx43 in PBS- and PF670462-injected retinas at 0 ($n = 7$), 6 ($n = 3$), 9 ($n = 6$), and 24 h ($n = 7$) in hypoxia. Samples from two separate animals are shown at each time point in *A*, *E*, and *G*. Data are presented as mean ± SEM. One-way ANOVA is used in *B*–*D*. Student's *t* test is used in *F*, *H*, and *J*. ns $P > 0.05$, *$P < 0.05$, **$P < 0.01$, ***$P < 0.001$, ****$P < 0.0001$.

we next determined whether prevention of Cx43 phosphorylation could protect astrocytes from hypoxia-induced damage and thereby promote reparative angiogenesis. In agreement with the results from $Cx43^{aKO}$ mice, we observed an increase in the population of astrocytes present in the avascular area of P14 $Cx43^{S3A}$ retinas compared with $Cx43^{WT}$ retinas, presumably due to obstruction of toxic signal trafficking among astrocytes (Fig. 7 *A* and *B*). Moreover, inhibition of Cx43 phosphorylation, either genetically in $Cx43^{S3A}$ retinas or pharmacologically upon intravitreal injection of PF670462, both accelerated revascularization of the retina (Fig. 7 *C*

and *D*) and suppressed the formation of neovascular tufts (Fig. 7 *C* and *E*) compared with controls ($Cx43^{WT}$) by P17. Finally, $Cx43^{S3A}$ retinas showed enhanced scotopic b-wave amplitudes in ERGs (Fig. 7 *F–H*), indicating recovery of neuroretinal function in these mice.

In summary, Cx43 phosphorylation by CK1δ during hypoxia causes augmentation of intercellular coupling via GJs channels, which negatively influences the density of astrocytes and the guided vascular growth.

Discussion

Current treatments for proliferative retinopathies are largely based on antiangiogenic agents such as VEGF antagonists (4, 50). Although anti-VEGF agents are effective, there are limitations associated with their use (51, 52). Therapies that successfully promote revascularization of the ischemic retina can offer a complementary approach for the treatment of retinopathies. We have demonstrated that restoration of functional vasculature to ischemic areas of the retina can be achieved by ablation of astrocytic Cx43 channels or inhibition of their phosphorylation by CK1δ at certain residues. The improvement in revascularization following Cx43 deletion or suppression of phosphorylation reduced retinal hypoxia and pathological neovascularization and strongly reversed decreases in neuronal function. In addition, we used an isoquinoline derivative (42) that inhibited Cx43 channels at low concentrations compared with other modulators and showed that pharmacological inhibition of Cx43 channels also promotes reparative angiogenesis. Our findings are also relevant for other diseases where vascular growth into ischemic areas is critical to prevent neuronal injury, such as stroke.

Furthermore, we describe a potential mechanism through which Cx43 impairs directional angiogenesis. Aberrant neovascularization is correlated with a hypoxia-induced decrease in astrocyte density, a phenomenon that has been consistently observed in animal models of retinopathy (7, 13, 14, 16, 18). Conversely, protecting astrocytes from hypoxia-induced damage using cell-based strategies, such as intravitreal injections of bone marrow-derived myeloid progenitor cells, astrocytes, or astrocyte-conditioned media, results in accelerated revascularization of the hypoxic tissue and reduced neovascularization (7, 8). However, the signals that initiate the hypoxia-induced degeneration of astrocytes have remained unclear. There is evidence that signaling pathways activated by proinflammatory cytokines such as TNFα play a role (53, 54). In addition to these primary pathways, our results indicate that the progressive loss of astrocytes in OIR is due to secondary cell death mediated by Cx43 channels. Deletion of Cx43 caused a decrease in apoptotic cell death and a significant increase in the density of astrocytes in the avascular areas of the retina. Consistent with bystander cell death propagated via GJ channels, functional studies indicated a large increase in the network of coupled astrocytes during the hypoxic phase of OIR. This increase in GJ-mediated coupling was specifically found in astrocytes located in the central avascular retina and occurred at time points before their degeneration. Preventing this increase in

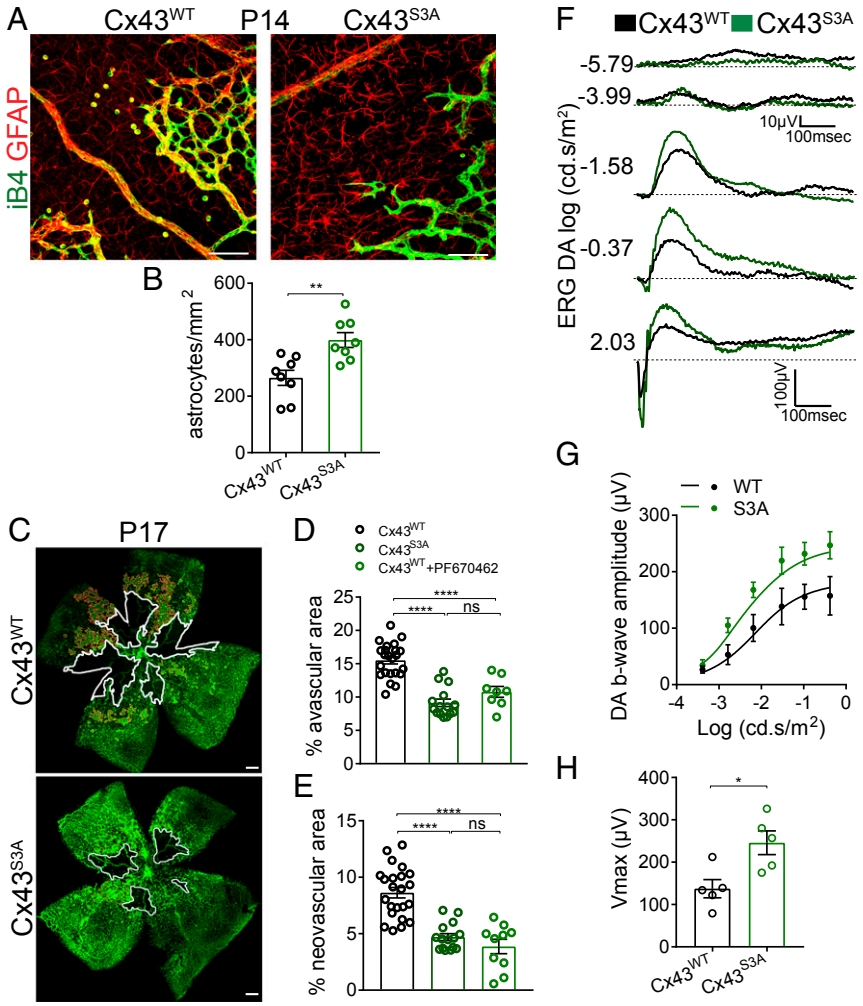

Fig. 7. Inhibition of CK1δ-mediated Cx43 phosphorylation rescues astrocytes, promotes reparative angiogenesis, and improves neuronal function. (*A*) Representative images of whole-mount $Cx43^{WT}$ and $Cx43^{S3A}$ retinas in OIR stained with isolectin (green) and anti-GFAP (red) at P14. (Scale bars: 100 μm.) (*B*) Quantification of astrocytes present in the avascular areas showed an ∼1.5-fold increase in their density in $Cx43^{S3A}$ retinas ($n = 8$) compared with $Cx43^{WT}$ ($n = 8$). (*C*) Representative images of whole-mount isolectin-stained $Cx43^{WT}$ and $Cx43^{S3A}$ retinas in OIR at P17. The borders of the avascular areas are outlined by white lines, and the neovascular tufts are marked by red lines. (Scale bars: 250 μm.) (*D* and *E*) Quantification of the avascular and neovascular areas at P17 in $Cx43^{WT}$ ($n = 23$), $Cx43^{S3A}$ ($n = 15$), and PF670462-treated ($n = 8$) mice. (*F*) Recordings of the a and b waves of scotopic ERGs at different stimulus intensities from $Cx43^{WT}$ and $Cx43^{S3A}$ mice at P28. Light intensities in log scot. cd s/m^2 are shown to the left of each trace. (*G*) Quantification of the scotopic b-wave amplitudes at different stimulus intensities ($n = 5$) showed significant improvement in neuronal function of $Cx43^{S3A}$ mice compared with $Cx43^{WT}$. Symbols represent the means ± SEM of the measured b-wave amplitudes. Lines represent the fit of the Naka Rushton equation to the data. (*H*) Quantification of the maximum response amplitude (V_{max}) in $Cx43^{WT}$ and $Cx43^{S3A}$ mice, estimated from the fitted curves in *G*. Data are presented as mean ± SEM. One-way ANOVA is used in *D* and *E*, and Student's *t* test is used in *B* and *H*. ns $P > 0.05$, *$P < 0.05$, **$P < 0.01$, ***$P < 0.001$, ****$P < 0.0001$.

CELL BIOLOGY

GJ coupling using inhibitors of Cx43 channels increased astrocytic density and promoted vascular remodeling.

Cx43 hemichannels also play an important role in secondary cell death in CNS ischemia (22, 25–27). Inhibition of Cx43 hemichannels reduces neuronal death and injury to the optic nerve in retinal ischemia and glaucoma (27, 40). However, our results do not support a role for Cx43 hemichannels in hypoxia-induced astrocyte loss in OIR. Thus, the relative contribution of hemichannels and/or GJ channels to secondary cell death is likely dependent on the nature of the insult.

A major advance made in this study is the finding that the deleterious actions of Cx43 in vivo are initiated by phosphorylation at specific serine residues in its C terminus. Phosphorylation of Cx43 soon after exposure to hypoxia was mediated by CK1δ and appeared to be limited to Cx43 expressed in astrocytes. CK1δ phosphorylates Cx43 on Ser325/328/330 during the transition of Cx43 from the plasma membrane into GJ plaques (47). Consistent with a role in GJ channel assembly, an antibody directed against Ser325/328/330-phosphorylated Cx43 recognizes the connexin protein only when it is present in GJ plaques (47, 48). Studies in cultured cells further indicate that either inhibition of CK1δ activity or substitution of the triplet of serines with alanines results in an accumulation of Cx43 in the nonjunctional membrane and a reduction in the strength of GJ coupling (48, 49) (also see *SI Appendix*, Fig. S8). Thus, the large increase in astrocytic GJ coupling observed in our study, which accompanied Cx43 phosphorylation, is in agreement with prior in vitro work. Moreover, in retinas injected with a CK1δ inhibitor, we found a reduction in both the hyperphosphorylated form of Cx43 and GJ astrocytic coupling in the central avascular retina. These results indicate that hypoxia promotes assembly of astrocytic Cx43 channels into GJ plaques via an increase in CK1δ activity. However, additional studies are required to identify the mechanisms by which CK1δ activation occurs in OIR. CK1δ could be directly activated by hypoxia-induced signaling. Alternately, CK1δ may be constitutively active, and so the increase in phosphorylation may be due to a reduction in the activity of a phosphatase, such as PP1 or PP2a, which are both known to localize with Cx43 in other tissues (55). Regardless of the underlying mechanism, preventing Cx43 phosphorylation by CK1δ reversed these hypoxia-induced changes and restored functional vasculature to ischemic areas of the retina in OIR.

Changes in Cx43 expression and function occur in early stages of diabetes and in models of retinal ischemia (40, 44, 56). Given the role of phosphorylation in the regulation of all aspects of the life cycle of Cx43, it will be of interest to examine whether such changes in these pathological settings are due to activation of specific kinase pathways. Identification of precise Cx43 phosphorylation events in these conditions might lead to the development of reagents with highly targeted modes of action. Our study highlights the feasibility of such an approach and shows that modulation of Cx43 phosphorylation can be a therapeutic avenue for treating ocular neovascular disorders.

Methods

Animals. All mouse strains were in C57BL/6J background. Animals of both sexes were used. WT C57BL/6J, $Cx43^{flox}$ (no. 008039), mGFAP-Cre (no. 012886), mTie2-Cre (no. 008863), and loxP-tdTomato Ai9 reporter mice (no. 007909) were purchased from Jackson Laboratories. Site-specific phosphorylation-deficient mice in which the serines 325 and 330 have been replaced with alanines and the serine 328 has been replaced with tyrosine (S325A/S328Y/S330A referred to as $Cx43^{S3A}$) were generated previously (57). All animal procedures were conducted in accordance with Association for Research in Vision and Ophthalmology statement regarding use of animals in vision research and were approved by the State University of New York Optometry Institutional Animal Care and Use Committee.

OIR. Mice pups were exposed to 75% oxygen for 5 d, from postnatal day 7 (P7) to P12, as described previously (28–30). At P12, mice returned to room air until P17. Hypoxia-induced neovascular tuft formation and revascularization were measured between P12 and P17. Retinal vasculatures were visualized using Alexa Fluor 488-conjugated IsolectinB4. The avascular retinal areas and the formation of neovascular tufts were quantified as described previously (28). The number of pixels in the vasoobliterated areas and in the neovascular tufts were counted and compared with the number of pixels of the total retinal area.

Intravitreal Injections. The Cx43 inhibitor SBO15 [compound 18 = 5-(4-phenoxybutoxy) isoquinoline in ref. 42] and the CK1δ inhibitor PF670462 (Tocris Bioscience) were diluted in PBS and injected intravitreally at various concentrations to the left eyes. The right eyes received PBS to serve as control (SHAM).

Immunofluorescence of Whole Mounts and Cryosections. For whole-mount preparations, eyes were enucleated, and retinas were isolated and fixed in 4% PFA solution for 1 h at room temperature. For vertical sections, retinas were cryoprotected, embedded in tissue freezing media (Electron Microscopy Science), and sliced vertically at 10 μm. Tissue was incubated with 5% (vol/vol) normal goat serum (Thermo Fisher Scientific) and 0.5% (vol/vol) TritonX (Millipore Sigma) in PBS for 1 h at room temperature and then with primary antibodies overnight at 4 °C and fluorescent secondary antibodies for 1 h at room temperature. Samples were mounted using mounting medium with DAPI (Vectashield; Vector Laboratories). Imaging was performed using a confocal microscope (Olympus FV1200 MPE).

Quantification of Astrocytic Density. Confocal microscopy images of whole mounts stained for GFAP and Isolectin were obtained at 20× and 60× magnifications. The number of astrocytes was counted manually, normalized to an area of 1 mm^2, and averaged across regions to obtain an astrocyte number for each retina. Astrocytes were identified as GFAP-expressing cells with DAPI-stained nuclei localized at the level of the superficial vascular plexus (DAPI staining is not shown for clarity purposes).

Western Blot. Retinas were dissected and homogenized in RIPA lysis buffer (Millipore Sigma) containing 1% protease inhibitor mixture (Millipore Sigma) and 1% phosphatase inhibitor mixture (Roche). Twenty micrograms of total retinal protein extract from individual mice were loaded in 10% acrylamide gels for electrophoresis. Separated proteins were transferred to nitrocellulose membranes (GE Healthcare), which were incubated overnight with appropriate primary antibodies. Fluorescent secondary antibodies were used for protein detection with an Odyssey imager (LI-COR Biosciences).

ERG Recordings and Data Analysis. Scotopic ERGs were recorded as described previously (58). ERG responses to brief white LED test flashes with intensities in the range of −6.7–2 log scotopic. cd s/m^2 were recorded using the Espion electrodiagnostic system (Diagnosys LLC). The a-wave amplitudes were measured from baseline to the maximum trough. The b-wave amplitudes were measured at their peak from the b-wave trough. OPs in the range of 70–300 Hz were extracted by digital filtering and quantified by summing the peak-to-trough amplitudes of the individual OPs within the first 100 ms. A generalized Naka Ruston equation (59) was fit to the data, and the maximum response amplitude (V_{max}), the slope (n), and the semisaturation constant (K) were estimated.

Dye Coupling. Retinas were dissected, transferred to filter papers (12-mm diameter cell culture inserts; Millipore Sigma), and kept in a chamber perfused with oxygenated bicarbonate extracellular buffer. A single astrocyte loaded with the GJ permeable tracer Neurobiotin (5 mg/mL) for 15 min in the whole-cell patch clamp configuration. Neurobiotin-filled astrocytes were visualized using Alexa Fluor 488-conjugated streptavidin and mouse anti-GFAP and counted manually in images obtained with confocal microscopy.

Dye Uptake. Retinas were incubated in PBS in the presence or absence of 300 μM Gap19 (Millipore Sigma) for 15 min at room temperature; 4 μM Ethidium Bromide (EtBr) (Millipore Sigma) were added to the solution for 10 min. Retinas were then processed for immunohistochemistry.

Statistics. Statistical analyses were performed using the Graph Pad Prism7 software. Results are presented as mean ± SEM. N values correspond to number of mice used in ERG experiments, and n values correspond to number of retinas used in all other experiments.

ACKNOWLEDGMENTS. This work was supported by NIH Grants EY007360 and EY026024 (to S.A.B.), NS100294 (to H.W.), GM55632 (to P.D.L.), and EY028170 (to M.S.).

1. Gilbert C, Awan H (2003) Blindness in children. *BMJ* 327:760–761.
2. Kempen JH, et al.; Eye Diseases Prevalence Research Group (2004) The prevalence of diabetic retinopathy among adults in the United States. *Arch Ophthalmol* 122: 552–563.
3. Cheung N, Mitchell P, Wong TY (2010) Diabetic retinopathy. *Lancet* 376:124–136.
4. Hartnett ME (2015) Pathophysiology and mechanisms of severe retinopathy of prematurity. *Ophthalmology* 122:200–210.
5. Sapieha P (2012) Eyeing central neurons in vascular growth and reparative angiogenesis. *Blood* 120:2182–2194.
6. Smith LE, Hard AL, Hellström A (2013) The biology of retinopathy of prematurity: How knowledge of pathogenesis guides treatment. *Clin Perinatol* 40:201–214.
7. Dorrell MI, et al. (2010) Maintaining retinal astrocytes normalizes revascularization and prevents vascular pathology associated with oxygen-induced retinopathy. *Glia* 58:43–54.
8. Ritter MR, et al. (2006) Myeloid progenitors differentiate into microglia and promote vascular repair in a model of ischemic retinopathy. *J Clin Invest* 116:3266–3276.
9. Connor KM, et al. (2007) Increased dietary intake of omega-3-polyunsaturated fatty acids reduces pathological retinal angiogenesis. *Nat Med* 13:868–873.
10. Joyal JS, et al. (2011) Ischemic neurons prevent vascular regeneration of neural tissue by secreting semaphorin 3A. *Blood* 117:6024–6035.
11. Wei Y, et al. (2015) Nrf2 in ischemic neurons promotes retinal vascular regeneration through regulation of semaphorin 6A. *Proc Natl Acad Sci USA* 112:E6927–E6936.
12. Xin X, et al. (2013) Hypoxic retinal Muller cells promote vascular permeability by HIF-1-dependent up-regulation of angiopoietin-like 4. *Proc Natl Acad Sci USA* 110: E3425–E3434.
13. Chan-Ling T, Stone J (1992) Degeneration of astrocytes in feline retinopathy of prematurity causes failure of the blood-retinal barrier. *Invest Ophthalmol Vis Sci* 33: 2148–2159.
14. Stone J, et al. (1996) Roles of vascular endothelial growth factor and astrocyte degeneration in the genesis of retinopathy of prematurity. *Invest Ophthalmol Vis Sci* 37: 290–299.
15. Gu X, et al. (2002) Effects of sustained hyperoxia on revascularization in experimental retinopathy of prematurity. *Invest Ophthalmol Vis Sci* 43:496–502.
16. Downie LE, Pianta MJ, Vingrys AJ, Wilkinson-Berka JL, Fletcher EL (2008) AT1 receptor inhibition prevents astrocyte degeneration and restores vascular growth in oxygen-induced retinopathy. *Glia* 56:1076–1090.
17. Bucher F, Stahl A, Agostini HT, Martin G (2013) Hyperoxia causes reduced density of retinal astrocytes in the central avascular zone in the mouse model of oxygen-induced retinopathy. *Mol Cell Neurosci* 56:225–233.
18. Weidemann A, et al. (2010) Astrocyte hypoxic response is essential for pathological but not developmental angiogenesis of the retina. *Glia* 58:1177–1185.
19. Yun JH, et al. (2016) Angiopoietin 2 induces astrocyte apoptosis via $\alpha v\beta 5$-integrin signaling in diabetic retinopathy. *Cell Death Dis* 7:e2101.
20. Ly A, et al. (2011) Early inner retinal astrocyte dysfunction during diabetes and development of hypoxia, retinal stress, and neuronal functional loss. *Invest Ophthalmol Vis Sci* 52:9316–9326.
21. Spray DC, et al. (2013) Gap junctions and bystander effects: Good Samaritans and executioners. *Wiley Interdiscip Rev Membr Transp Signal* 2:1–15.
22. Freitas-Andrade M, Naus CC (2016) Astrocytes in neuroprotection and neurodegeneration: The role of connexin43 and pannexin1. *Neuroscience* 323:207–221.
23. Perez Velazquez JL, Kokarovtseva L, Sarbaziha R, Jeyapalan Z, Leshchenko Y (2006) Role of gap junctional coupling in astrocytic networks in the determination of global ischaemia-induced oxidative stress and hippocampal damage. *Eur J Neurosci* 23:1–10.
24. Takahashi DK, Vargas JR, Wilcox KS (2010) Increased coupling and altered glutamate transport currents in astrocytes following kainic-acid-induced status epilepticus. *Neurobiol Dis* 40:573–585.
25. Bennett MV, et al. (2012) Connexin and pannexin hemichannels in inflammatory responses of glia and neurons. *Brain Res* 1487:3–15.
26. Giaume C, Leybaert L, Naus CC, Sáez JC (2013) Connexin and pannexin hemichannels in brain glial cells: Properties, pharmacology, and roles. *Front Pharmacol* 4:88.
27. Danesh-Meyer HV, Zhang J, Acosta ML, Rupenthal ID, Green CR (2016) Connexin43 in retinal injury and disease. *Prog Retin Eye Res* 51:41–68.
28. Connor KM, et al. (2009) Quantification of oxygen-induced retinopathy in the mouse: A model of vessel loss, vessel regrowth and pathological angiogenesis. *Nat Protoc* 4: 1565–1573.
29. Smith LE, et al. (1994) Oxygen-induced retinopathy in the mouse. *Invest Ophthalmol Vis Sci* 35:101–111.
30. Stahl A, et al. (2010) The mouse retina as an angiogenesis model. *Invest Ophthalmol Vis Sci* 51:2813–2826.
31. Solan JL, Lampe PD (2007) Key connexin 43 phosphorylation events regulate the gap junction life cycle. *J Membr Biol* 217:35–41.
32. Musil LS, Cunningham BA, Edelman GM, Goodenough DA (1990) Differential phosphorylation of the gap junction protein connexin43 in junctional communication-competent and -deficient cell lines. *J Cell Biol* 111:2077–2088.
33. Solan JL, Lampe PD (2009) Connexin43 phosphorylation: Structural changes and biological effects. *Biochem J* 419:261–272.
34. Zahs KR, Newman EA (1997) Asymmetric gap junctional coupling between glial cells in the rat retina. *Glia* 20:10–22.
35. Akopian A, et al. (2014) Gap junction-mediated death of retinal neurons is connexin and insult specific: A potential target for neuroprotection. *J Neurosci* 34: 10582–10591.
36. Ceelen PW, Lockridge A, Newman EA (2001) Electrical coupling between glial cells in the rat retina. *Glia* 35:1–13.
37. Dorfman AL, Polosa A, Joly S, Chemtob S, Lachapelle P (2009) Functional and structural changes resulting from strain differences in the rat model of oxygen-induced retinopathy. *Invest Ophthalmol Vis Sci* 50:2436–2450.
38. Fulton AB, Hansen RM, Moskowitz A, Akula JD (2009) The neurovascular retina in retinopathy of prematurity. *Prog Retin Eye Res* 28:452–482.
39. Wang N, et al. (2013) Connexin targeting peptides as inhibitors of voltage- and intracellular Ca2+-triggered Cx43 hemichannel opening. *Neuropharmacology* 75: 506–516.
40. Danesh-Meyer HV, et al. (2012) Connexin43 mimetic peptide reduces vascular leak and retinal ganglion cell death following retinal ischaemia. *Brain* 135:506–520.
41. Li X, et al. (2015) Inhibition of connexin43 improves functional recovery after ischemic brain injury in neonatal rats. *Glia* 63:1553–1567.
42. Bodendiek SB, Mahieux C, Hänsel W, Wulff H (2009) 4-Phenoxybutoxy-substituted heterocycles–A structure-activity relationship study of blockers of the lymphocyte potassium channel Kv1.3. *Eur J Med Chem* 44:1838–1852.
43. Abudara V, et al. (2014) The connexin43 mimetic peptide Gap19 inhibits hemichannels without altering gap junctional communication in astrocytes. *Front Cell Neurosci* 8:306.
44. Sato T, Haimovici R, Kao R, Li AF, Roy S (2002) Downregulation of connexin 43 expression by high glucose reduces gap junction activity in microvascular endothelial cells. *Diabetes* 51:1565–1571.
45. Musil LS, Goodenough DA (1991) Biochemical analysis of connexin43 intracellular transport, phosphorylation, and assembly into gap junctional plaques. *J Cell Biol* 115: 1357–1374.
46. Falk MM, Bell CL, Kells Andrews RM, Murray SA (2016) Molecular mechanisms regulating formation, trafficking and processing of annular gap junctions. *BMC Cell Biol* 17:22.
47. Cooper CD, Lampe PD (2002) Casein kinase 1 regulates connexin-43 gap junction assembly. *J Biol Chem* 277:44962–44968.
48. Lampe PD, Cooper CD, King TJ, Burt JM (2006) Analysis of connexin43 phosphorylated at S325, S328 and S330 in normoxic and ischemic heart. *J Cell Sci* 119:3435–3442.
49. Remo BF, et al. (2011) Phosphatase-resistant gap junctions inhibit pathological remodeling and prevent arrhythmias. *Circ Res* 108:1459–1466.
50. Aiello LP, et al. (1995) Suppression of retinal neovascularization in vivo by inhibition of vascular endothelial growth factor (VEGF) using soluble VEGF-receptor chimeric proteins. *Proc Natl Acad Sci USA* 92:10457–10461.
51. Saint-Geniez M, et al. (2008) Endogenous VEGF is required for visual function: Evidence for a survival role on müller cells and photoreceptors. *PLoS One* 3:e3554.
52. Holz FG, et al.; SUSTAIN Study Group (2011) Safety and efficacy of a flexible dosing regimen of ranibizumab in neovascular age-related macular degeneration: The SUSTAIN study. *Ophthalmology* 118:663–671.
53. Gardiner TA, et al. (2005) Inhibition of tumor necrosis factor-alpha improves physiological angiogenesis and reduces pathological neovascularization in ischemic retinopathy. *Am J Pathol* 166:637–644.
54. Stevenson L, et al. (2010) Reduced nitro-oxidative stress and neural cell death suggests a protective role for microglial cells in TNFalpha-/- mice in ischemic retinopathy. *Invest Ophthalmol Vis Sci* 51:3291–3299.
55. Ai X, Pogwizd SM (2005) Connexin 43 downregulation and dephosphorylation in nonischemic heart failure is associated with enhanced colocalized protein phosphatase type 2A. *Circ Res* 96:54–63.
56. Bobbie MW, et al. (2010) Reduced connexin 43 expression and its effect on the development of vascular lesions in retinas of diabetic mice. *Invest Ophthalmol Vis Sci* 51: 3758–3763.
57. Huang GY, et al. (2011) Evaluating the role of connexin43 in congenital heart disease: Screening for mutations in patients with outflow tract anomalies and the analysis of knock-in mouse models. *J Cardiovasc Dis Res* 2:206–212.
58. Akopian A, Kumar S, Ramakrishnan H, Viswanathan S, Bloomfield SA (2016) Amacrine cells coupled to ganglion cells via gap junctions are highly vulnerable in glaucomatous mouse retinas. *J Comp Neurol*, 10.1002/cne.24074.
59. Joshi NR, Ly E, Viswanathan S (2017) Intensity response function of the photopic negative response (PhNR): Effect of age and test-retest reliability. *Doc Ophthalmol* 135:1–16.